VLA SCIENTIFIC MEMORANDUM #3

Robert H. MacPhie *

May 1967

THE USE OF SPACE-FREQUENCY EQUIVALENCE IN LONG-BASELINE INTERFEROMETERS

NATIONAL RADIO ASTRONOMY OBSERVATORY

---

* The author is Associate Professor of Electrical Engineering at the University of Waterloo, Waterloo, Ontario, Canada

THE USE OF SPACE-FREQUENCY EQUIVALENCE IN LONG-BASELINE INTERFEROMETERS

ABSTRACT

Space-frequency equivalence theory is applied to long-baseline interferometers used for aperture synthesis in radio astronomy. A double sideband correlation interferometer, with isotropic elements, rectangular bandwidth B(Hz), intermediate frequency ω_1, radio frequency ω_o, and a baseline z_o, is identical in performance to a monochromatic interferometer (bandwidth approaching zero) whose baseline is z_o and whose "elements" are as follows:

a) A uniformly weighted linear aperture of length $2L = 2\frac{\pi B}{\omega_o} z_o$,

b) A simple two-element interferometer, element separation $2\ell = 2\frac{\omega_1}{\omega_o} z_o$.

At sufficiently long baselines the interferometer's spatial frequency passband, proportional to the product of the baseline and temporal frequency bandwidth, extends over many sampling points used in conventional aperture synthesis. With the baseline held fixed, the spatial frequency spectrum at these points can be deduced from a series of measured outputs obtained by incremental time delays ($\Delta\tau = \frac{1}{2B}$) in the IF of the cross-correlator.

Because the spatial frequency passband is directly proportional to the baseline, one can exponentially increase the baseline intervals without loss of spatial frequency information and significantly reduce the total number of the baselines needed for aperture synthesis.

I. INTRODUCTION

It has been known for at least a decade that there is an equivalence relation between antenna systems operating with different bandwidths and spatial geometries. According to Koch and Stone [1], a simple two-element interferometer, which operates over a wide band of frequencies, is equivalent in performance to a multi-element array operating over a very narrow frequency band.

In radio astronomy two-element interferometers have been used for many years [2,3]. In particular this has resulted in the method of aperture synthesis due to Ryle [4], whereby very large arrays have been simulated by a series of measurements with a two-element interferometer, measurements taken at uniform intervals in a very large, but otherwise empty, aperture.

Interferometer methods have also been proposed for the Very Large Array (VLA) of the National Radio Astronomy Observatory [5]. The 36 parabolic antennas of the array are located on the arms of an equiangular wye configuration, each arm being 21 kilometers in length. The output from each array element, with a circular aperture of 25 meters, is cross-correlated with the outputs from all the others, forming 1/2 (36) (35) = 630 correlations. In effect there are 630 distinct two-element interferometers in the system.

Now the proposed bandwidth of the VLA is 50 MHz at an operating frequency of 2695 MHz--a fractional bandwidth of 1.85 percent. For most applications this is sufficiently narrow that in the system pattern analysis one could assume single-frequency operation. However, as will be shown,

this bandwidth, when used with very long baseline interferometers, causes signal dispersion, and in the absence of additional processing by the cross-correlator a loss of information will occur.

In this paper the effect of bandwidth on the operation of a simple two-element interferometer is analyzed from the space-frequency viewpoint to obtain an equivalent long-baseline interferometer of more complicated geometry but operating at a single frequency. At long baselines the spatial frequency response of a double sideband interferometer [6] broadens into two passbands on either side of the nominal frequency determined by the baseline. The passbands may be many of the original sampling intervals in width. It will be shown that one can increase the baseline intervals for large separation between elements without loss of spatial frequency information. With the baseline held fixed, the interferometer output is varied by uniform discrete increments of the time-delay in the cross-correlator; from these outputs one can deduce the spatial frequency response at the sampling intervals within the interferometer passbands.

With a broadband interferometer there is a reduction in the number of baselines at which measurements need be made, but at each of the longer baselines more measurements are needed. With interferometers such as those of the VLA, whose 25 meter dishes are not easily moved, it should be far easier to vary the correlator time delays than to vary the interferometer baselines, and a saving in time as well as money should result.

However, the most compelling reason for increasing the sampling interval at long baselines is that it prevents the overlap of the broadening

passbands of the interferometers and consequently prevents serious distortion of the spatial frequency spectrum which is measured.

II. THE DOUBLE-SIDEBAND CORRELATION INTERFEROMETER

Let us consider a simple interferometer with identical isotropic elements located z_o meters apart on the z-axis (the interferometer baseline) of the coordinate system shown in Figure 1. We assume that a plane wave is incident from the direction θ. The outputs from the two elements are identical (in the absence of noise) except for a time delay τ due to the different arrival time of the wave at the two elements. The correlation of these two signals is described in Appendix A. If the IF filter characteristics are rectangular, with a center frequency ω_1 and bandwidth B(Hz), and if the RF frequency is ω_o (as shown in Figure 2), then the interferometer output becomes

$$R'(\tau) = \left\{ \frac{\sin \pi B\tau}{\pi B\tau} \cos \omega_1 \tau \right\} \cos \omega_o \tau \ , \tag{1}$$

where $\tau = \frac{\cos \theta}{c} z_o$, and c is the velocity of light.

Now the factor in the curly brackets in Equation (1), the instrument factor, varies much more slowly with τ than does the true interferometer factor, $\cos \omega_o \tau$. It acts as an envelope of the latter, and for the important case when $\omega_1 = \pi B$ the instrument factor simplifies to

$$\frac{\sin \left(\frac{2\pi B}{c} z_o \cos \theta \right)}{\frac{2\pi B}{c} z_o \cos \theta} = \frac{\sin \frac{2\pi B}{\omega_o} z_o u}{\frac{2\pi B}{\omega_o} z_o u} \ , \tag{2}$$

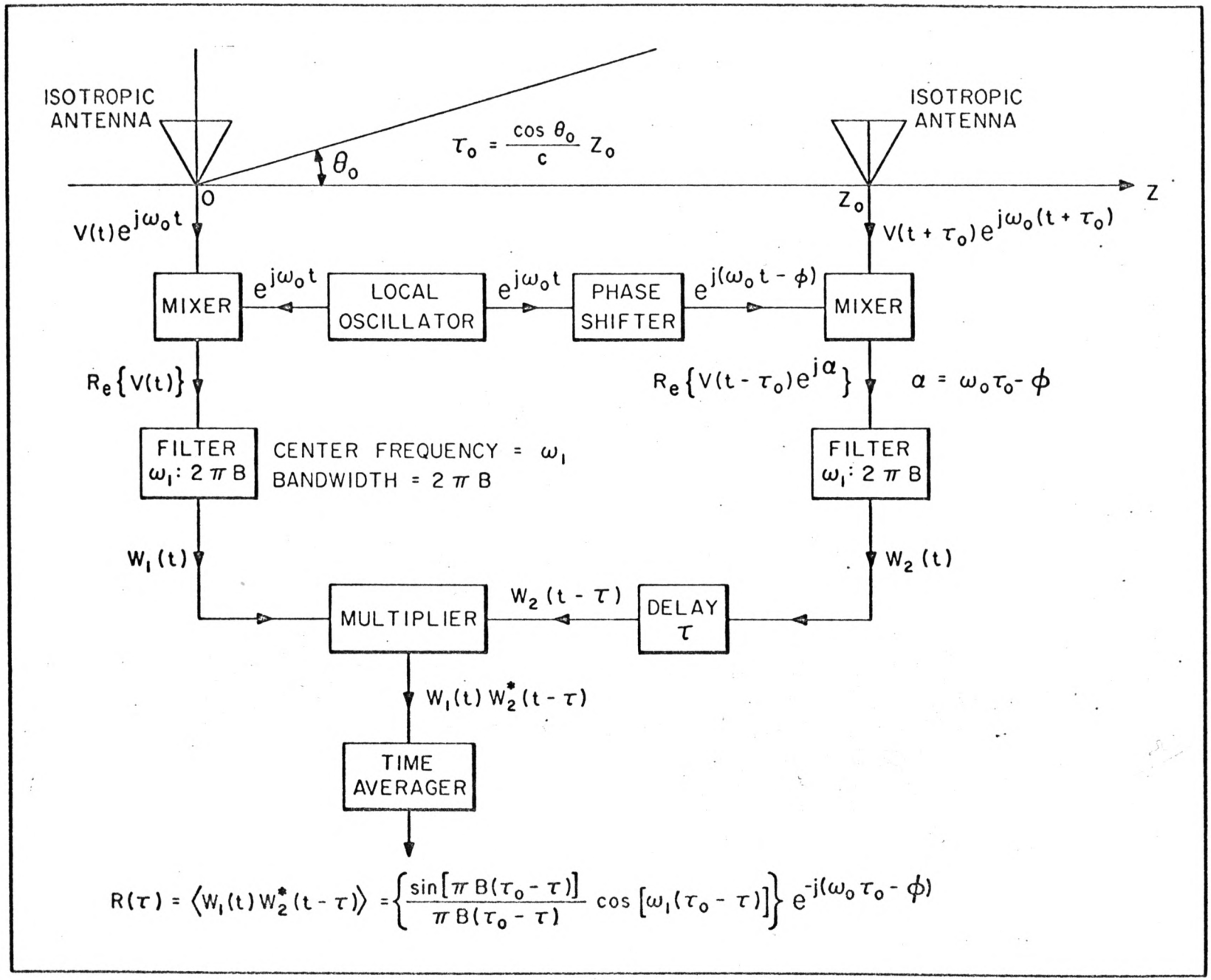

Figure 1: Double-sideband correlation interferometer

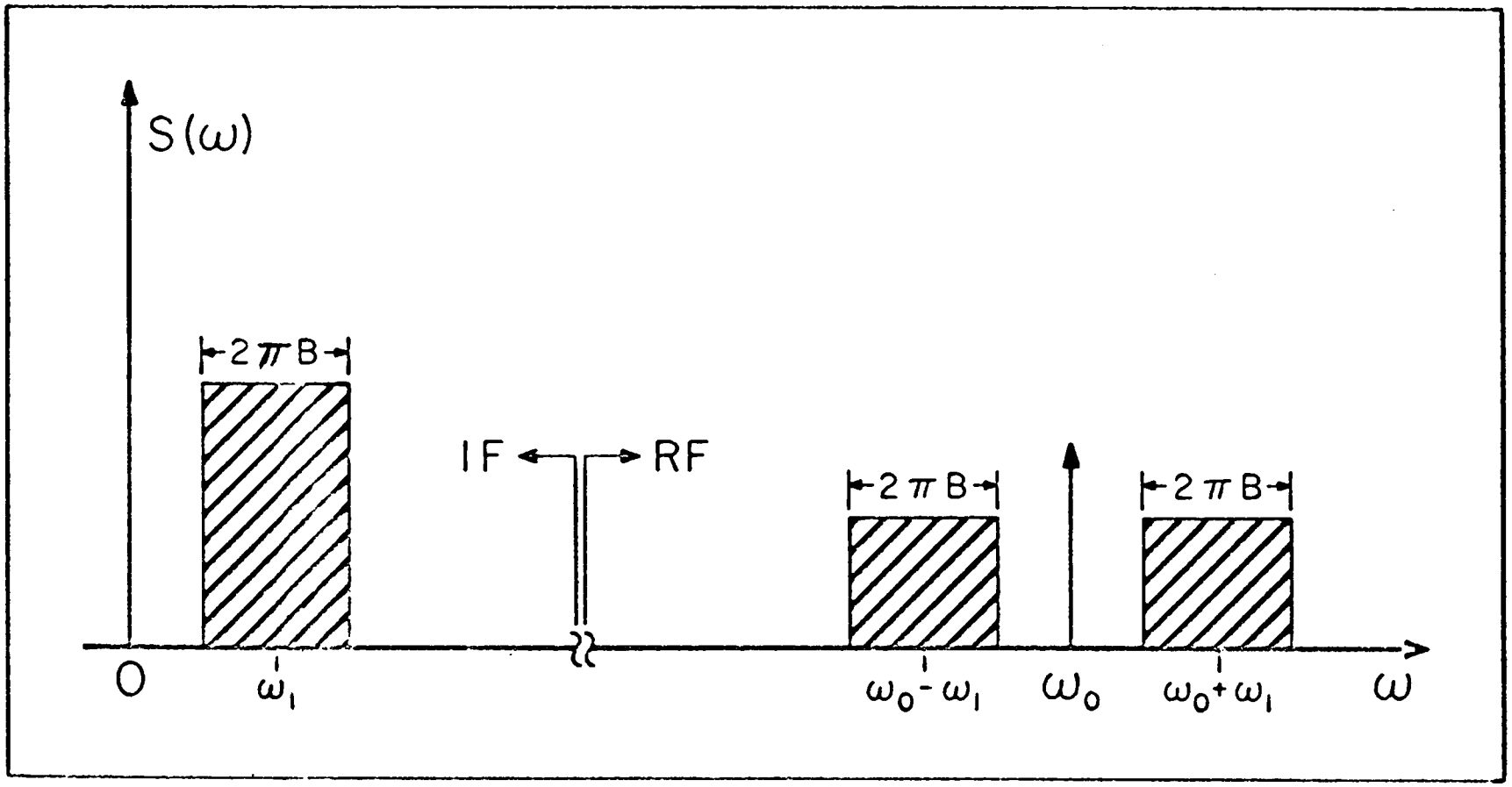

Figure 2: Power spectra of the correlation interferometer

where $u = \frac{\omega_o}{c} \cos\theta$.

The variations of this "bandwidth pattern" as a function of u is illustrated in Figure 3. Clearly there is a suppression of the response to sources away from the direction $u = 0$ or $\theta = \frac{\pi}{2}$. This suppression is proportional to the <u>product</u> of the bandwidth B and the baseline z_o of the interferometer. Roughly speaking, only sources falling within the main lobe of the pattern (for which $|u| \leq \frac{\omega_o}{2Bz_o}$) will be observed by the interferometer.

III. SPATIAL FREQUENCY ANALYSIS

If we let u be the pattern variable and z be the spatial frequency variable (the product uz is in radians), then the pattern of the double-sideband interferometer is

$$P(u) = \left\{ \frac{\sin\left(\frac{\pi B}{\omega_o} z_o u\right)}{\frac{\pi B}{\omega_o} z_o u} \cos\left(\frac{\omega_1}{\omega_o} z_o u\right) \right\} \cos(z_o u). \qquad (3)$$

The spatial frequency spectrum is the Fourier transform of P(u)

$$p(z) = \int_{-\infty}^{\infty} P(u) e^{-juz}\, du = \mathcal{F}\{P(u)\}.$$

By the convolution theorem

$$p(z) = \mathcal{F}\left\{ \frac{\sin\left(\frac{\pi B}{\omega_o} z_o u\right)}{\frac{\pi B}{\omega_o} z_o u} \right\} * \mathcal{F}\left\{ \cos\left(\frac{\omega_1}{\omega_o} z_o u\right) \right\} * \mathcal{F}\{\cos(z_o u)\} \qquad (4)$$

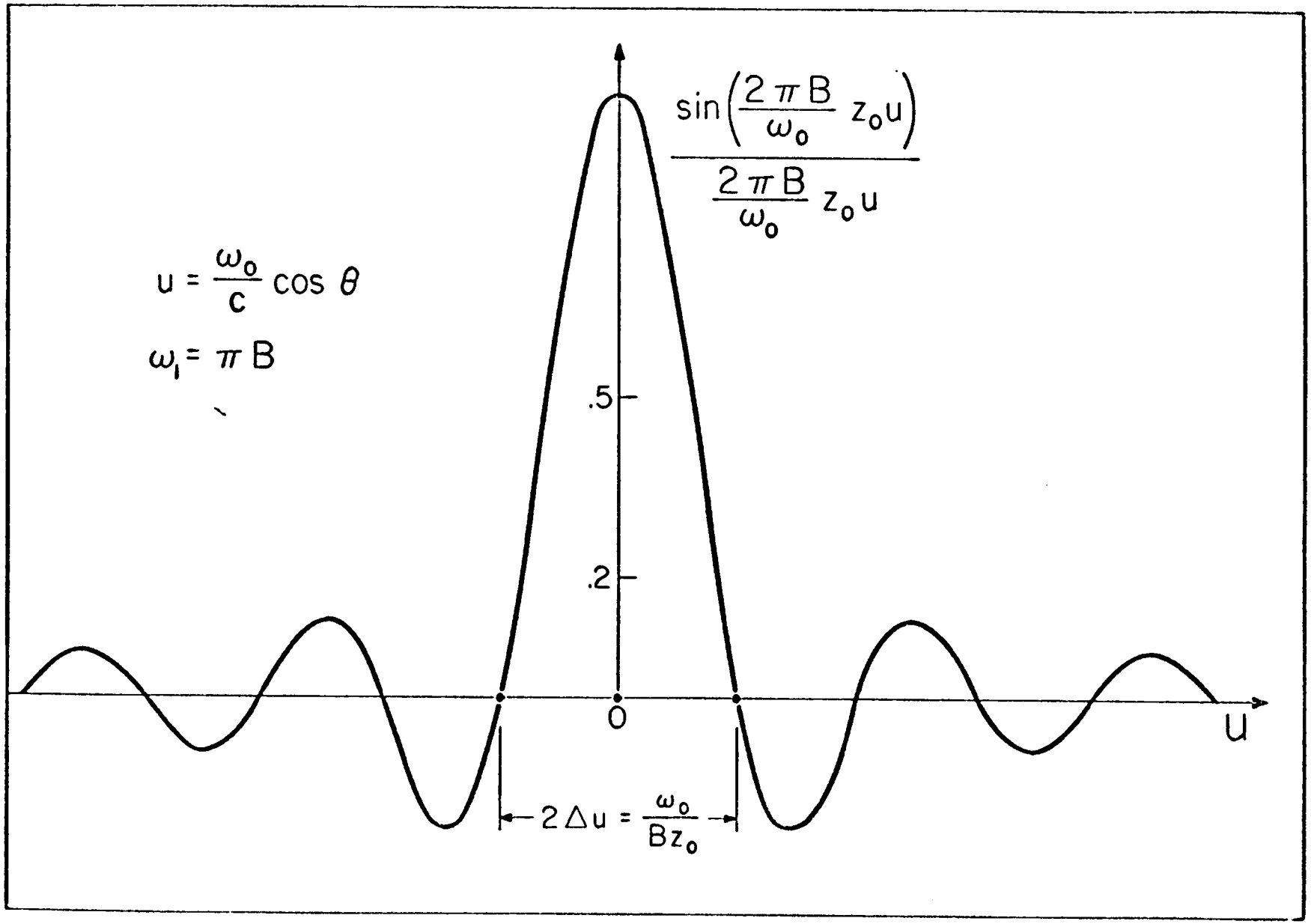

Figure 3: Bandwidth pattern

where $\ast$ indicates convolution. The transforms of

$$\frac{\sin\left(\frac{\pi B}{\omega_o} z_o u\right)}{\frac{\pi B}{\omega_o} z_o u}, \quad \cos\left(\frac{\omega_1}{\omega_o} z_o u\right), \quad \text{and} \quad \cos(z_o u),$$

are shown in Figure 4(a) and the spatial frequency spectrum p(z) is shown in Figure 4(b).

$$p(z) = \frac{\omega_o}{8\pi B z_o}, \quad \text{if} \quad \left||z| - \left(1 \pm \frac{\omega_1}{\omega_o}\right) z_o\right| \leq \frac{\pi B}{\omega_o} z_o \tag{5}$$

$$= 0 \quad , \text{otherwise.}$$

Now as is well known, the interferometer output R(u) is the convolution of P(u) and the brightness temperature T(u). Thus, the spatial frequency spectrum of the output is

$$r(z) = p(z)t(z), \tag{6}$$

where

$$t(z) = \int_{-\infty}^{\infty} T(u)e^{juz}\, du = \mathcal{F}\{T(u)\}$$

is the spatial frequency spectrum of T(u). In the case of a point source at $u = u_o$, we get

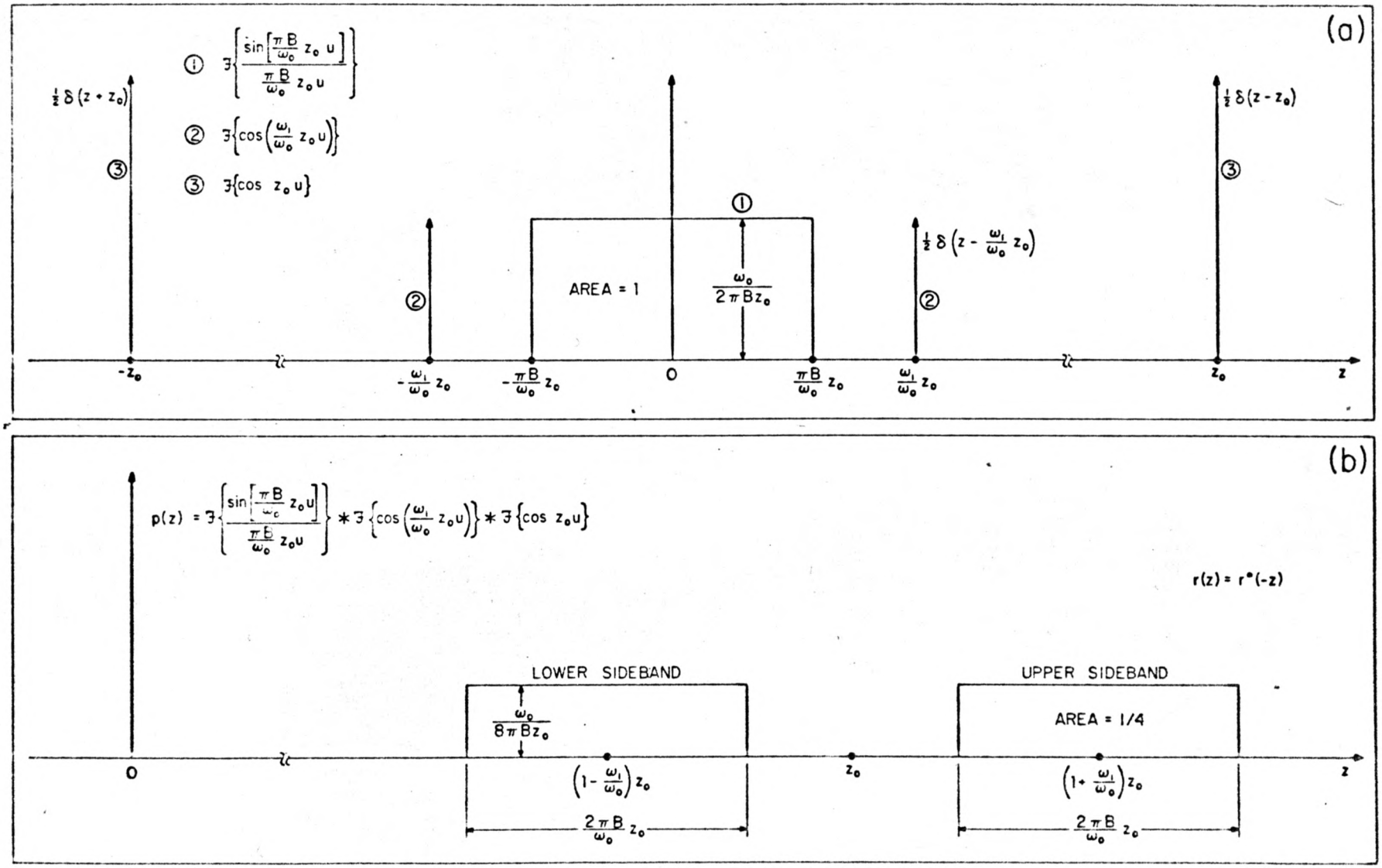

Figure 4: Spatial frequency spectra of (a) interferometer factor patterns and of (b) interferometer product pattern.

$$r(z) = p(z)\, e^{ju_o z}$$

$$= \frac{\omega_o}{8\pi B z_o}\, e^{ju_o z}, \text{ for } \left| |z| - \left(1 \pm \frac{\omega_1}{\omega_o}\right) z_o \right| \leq \frac{\pi B}{\omega_o}\, z_o, \qquad (7)$$

$$= 0, \text{ otherwise.}$$

Consequently, except for the constant factor $\frac{\omega_o}{8\pi B z_o}$, the output spectrum is equal to the spatial frequency spectrum of the brightness temperature distribution, over the passband of the interferometer. This, of course, is the principal solution spectrum of Bracewell and Roberts [6].

The effect of the bandwidth B and of the intermediate frequency ω_1 is clearly shown in Figure 4(b). With a double-sideband interferometer one obtains two sidebands of width $\frac{2\pi B}{\omega_o}\, z_o$, symmetrically located on either side of the original baseline position z_o; the separation between sidebands is $2\frac{\omega_1}{\omega_o}\, z_o$. Note that if $\frac{\omega_1}{\pi B} > 1$, as is the case in Figure 4, then there is no spatial frequency response of the system at the nominal baseline distance z_o.

IV. AN EQUIVALENT CORRELATION INTERFEROMETER OPERATING AT A SINGLE FREQUENCY

We now seek a monochromatic interferometer operating at the original center frequency ω_o which has the same performance characteristics as the double sideband system. Specifically the new system's pattern should also be given by

$$P(u) = \left\{ \frac{\sin\left[\frac{\pi B}{\omega_o} z_o u\right]}{\frac{\pi B}{\omega_o} z_o u} \cos\left(\frac{\omega_1}{\omega_o} z_o u\right) \right\} \cos z_o u. \qquad (8)$$

Inspection of the first factor in the curly bracket reveals that its variation with u is identical to the pattern variation of a uniformly illuminated linear aperture of length 2L:

$$A(u) = \frac{\sin Lu}{Lu} . \tag{9}$$

Similarly the second factor is identical to the pattern of a simple interferometer with element spacing 2ℓ:

$$B(u) = \cos \ell u . \tag{10}$$

If these antennas are used as the elements of a correlation interferometer, as shown in Figure 5, then the pattern, when the element separation is z_o, becomes

$$P(u) = \text{Re} \left\{ A(u)B^*(u)e^{-jz_o u} \right\} = \left\{ \frac{\sin Lu}{Lu} \cos \ell u \right\} \cos z_o u, \tag{11}$$

where "Re ...," indicates "The real part of ....", and B* is the complex conjugate of B.

Comparing (8) and (11) we see that the two patterns will be identified if we set

$$L = \frac{\pi B}{\omega_o} z_o, \qquad \ell = \frac{\omega_1}{\omega_o} z_o. \tag{12}$$

It is important to note that both L and ℓ are <u>directly proportional</u> to the interferometer baseline z_o. For very short baselines the two distances

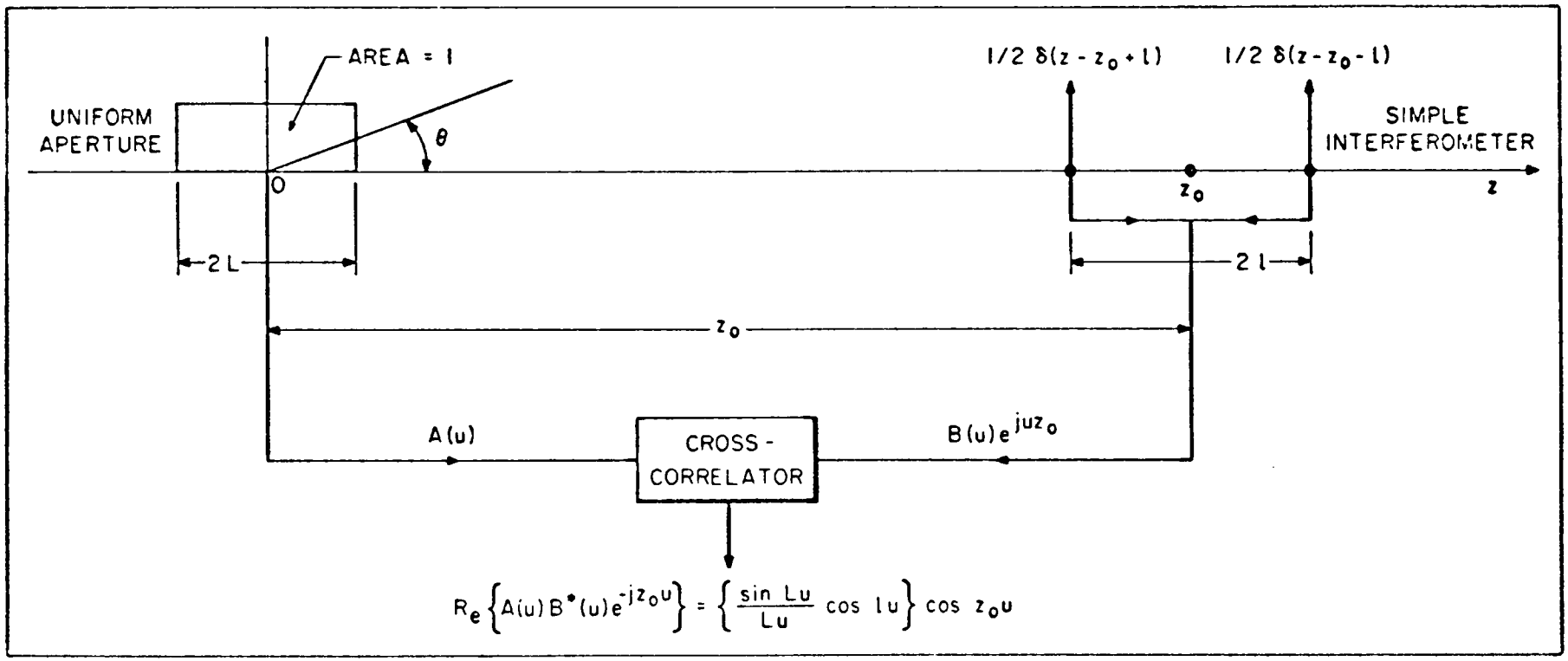

Figure 5: Equivalent monochromatic interferometer.

are much less than a wavelength λ_o and the system reduces to a simple two-element interferometer with essentially isotropic elements. This case is illustrated in Figure 6(a) where the spatial frequency response is shown. Figures 6(b) and 6(c) indicate the equivalent spatial frequency responses for intermediate and long baselines, respectively. Figure 6 also illustrates the fact that as the spatial frequency response broadens with increasing baselines, its intensity, at any point in the passbands, decreases in such a fashion that the area of each passband remains constant at 1/4. The total area, including the passbands at negative frequencies, is unity.

V. MODIFICATION OF INTERFEROMETER SAMPLING INTERVALS DUE TO BANDWIDTH

As is well-known, measurements with radio interferometers are made at discrete intervals along the baseline passing through the two elements. If the elements are isotropic, it is necessary to measure the field coherence at baseline intervals of one-half wavelength. However, for sufficiently long baselines the spatial frequency passbands of width $\frac{2\pi B}{\omega_o} z_o$ will themselves extend over many RF wavelengths and in effect make many simultaneous samplings of the field coherence. Our task is to devise a sampling method which takes advantage of this broadening of the spatial frequency passband as the baseline increases.

To simplify the analysis let us consider the important case when $\omega_1 = \pi B$ and the two spatial frequency sidebands have no intervening gap. Then the spatial frequency response of the interferometer, for a series of

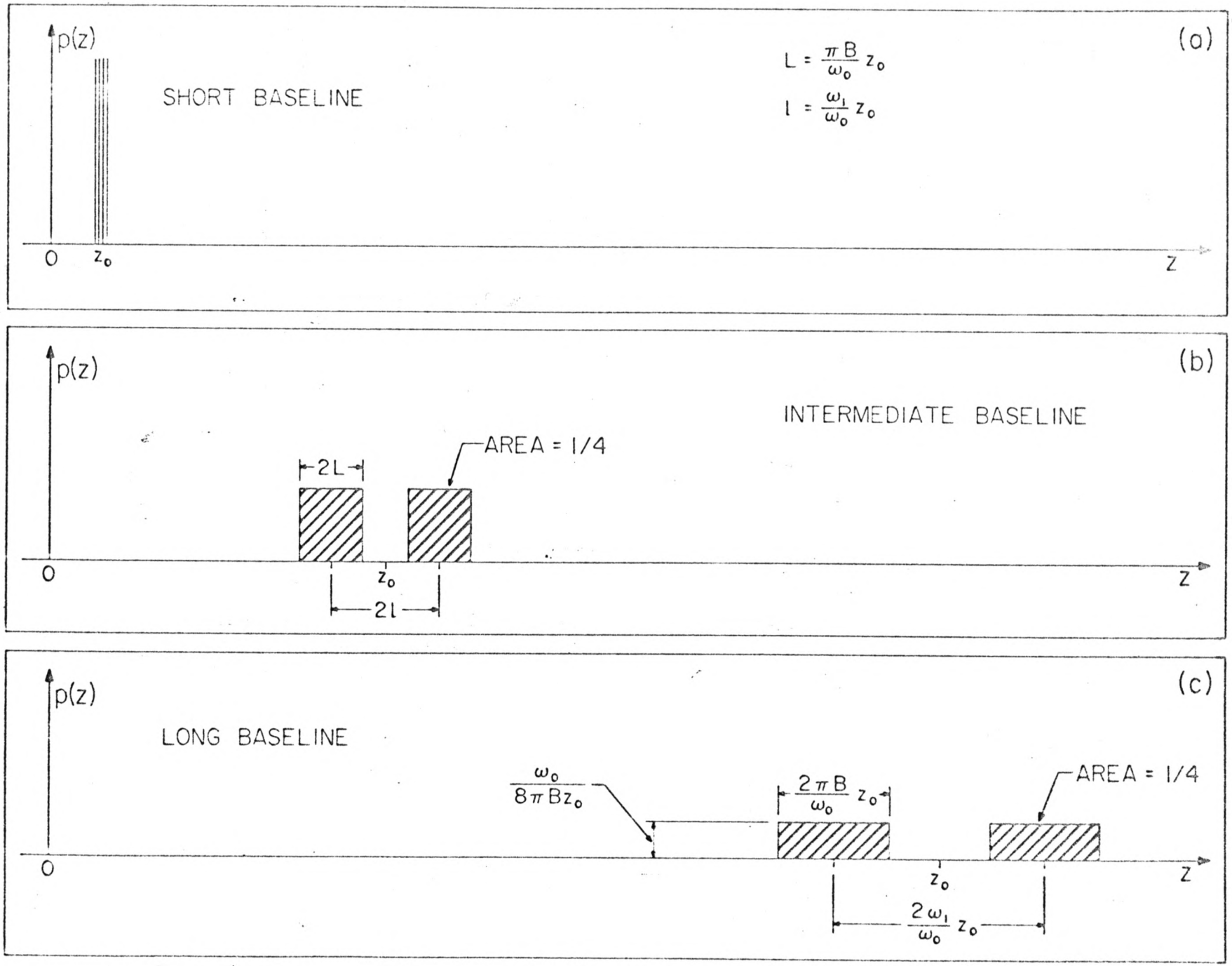

Figure 6: Spatial frequency response for (a) short baseline, (b) intermediate baseline and (c) long baseline.

measurements at half wavelength intervals, is shown in Figure 7(a). The ratio of bandwidth to operating frequency, which we define as $\alpha = \frac{2\pi B}{\omega_o}$, is 0.10. Note that the broadening of the spatial frequency passbands as z increases eventually results in an overlap (shown hatched) between the responses at $z = \frac{5}{2}\ \lambda_o$ and $z = 3\ \lambda_o$. This overlapping of responses becomes progressively greater at longer baselines. In order to prevent such redundancy, one could increase the last interferometer baseline from $3\ \lambda_o$ to $3.06\ \lambda_o$; then the two passbands would just touch (at $z = 2.75\ \lambda_o$) with no redundancy and no intervening gap.

It would also be necessary to increase the baselines of all measurements of the higher spatial frequencies to prevent overlap. This results in the staircase characteristic shown in Figure 7(b). It is not difficult to show that the longer interferometer spacings are related to the last unshifted spacing of $\bar{n}\ \frac{\lambda_o}{2}$ by the formula

$$z_n = \left(\frac{1+\alpha}{1-\alpha}\right)^{(n-\bar{n})}\ \bar{n}\,\frac{\lambda_o}{2}\ , \quad \text{where } \alpha = \frac{2\pi B}{\omega_o}\ , \tag{13}$$

and that

$$\bar{n} = \left[\frac{1-\alpha}{2\alpha}\right], \tag{14}$$

where [x] is the first integer greater than x.

In the case illustrated in Figure 7, $\bar{n} = 5$, and for n = 6,7,8 we have $z_6 = 3.06\ \lambda_o$, $z_7 = 3.74\ \lambda_o$, $z_8 = 4.57\ \lambda_o$. These locations are shown

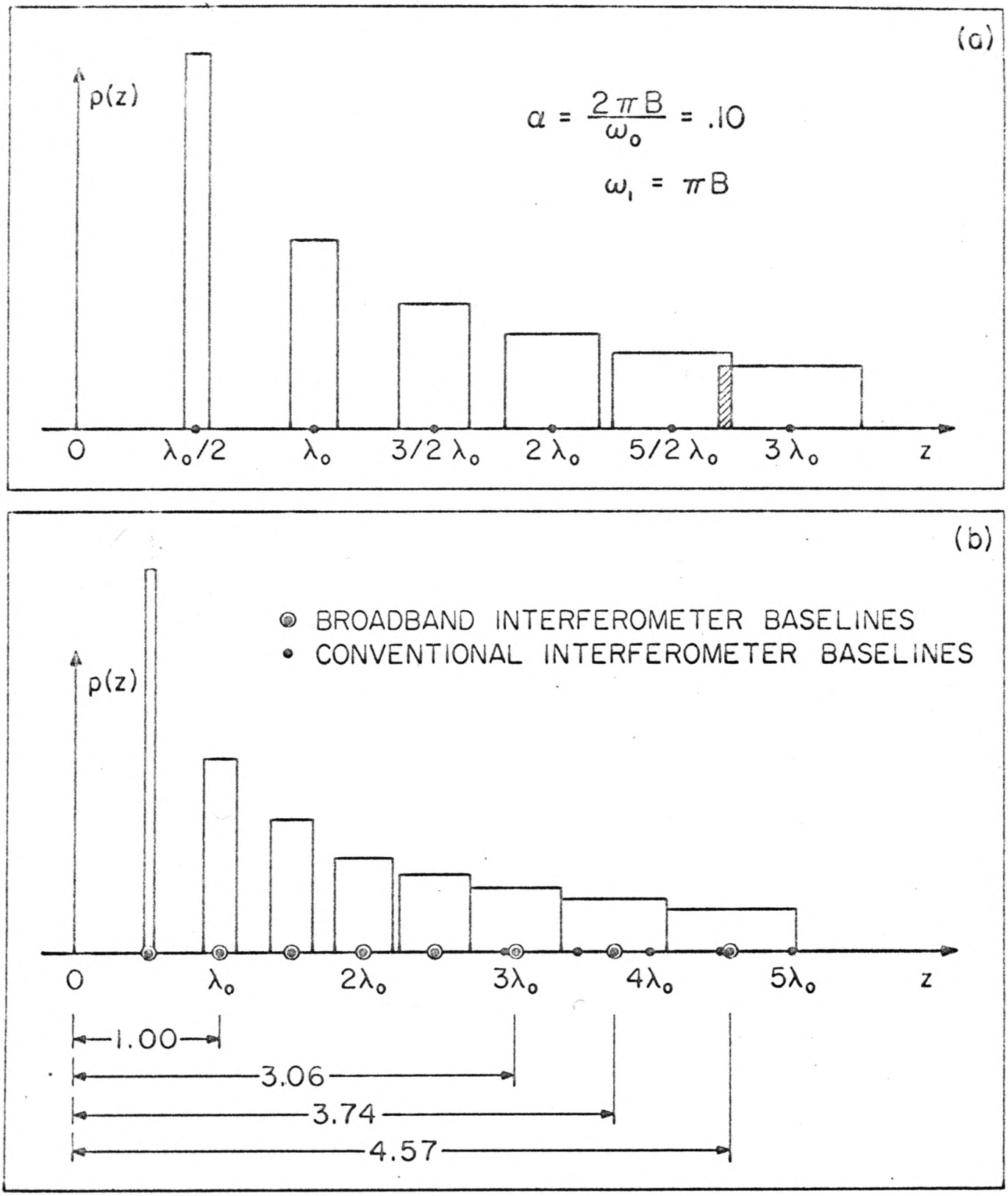

Figure 7: (a) Spatial frequency overlapping at long baselines
(b) Modification of baselines to prevent overlapping.

in Figure 7(b). Note that in the interval of five wavelengths, which for single frequency operation requires ten interferometer baselines, there are only eight baselines for the broadband system.

More generally, if the double sideband interferometer has a relative bandwidth of $\alpha = \frac{2\pi B}{\omega_o}$, and an intermediate frequency of $\omega_1 = \pi B$, then for N interferometer baselines the total spatial frequency coverage Z_N is given by

$$Z_N = (1 + \alpha) z_N = (1 + \alpha) \left(\frac{1 + \alpha}{1 - \alpha}\right)^{\left(N - \left[\frac{1 - \alpha}{2\alpha}\right]\right)} \left[\frac{1 - \alpha}{2\alpha}\right] \frac{\lambda_o}{2}. \qquad (15)$$

The number of half-wavelength intervals in Z_N is $M = 2 \frac{Z_N}{\lambda_o}$ and is plotted as a function of N, with α as a parameter, in Figure 8. The straight solid line is the monochromatic limit for which $\alpha = 0$. The curves for $\alpha > 0$ show that as the bandwidth increases the number of half wavelength intervals M rapidly becomes much larger than the number of the individual baselines N. This results in a much larger maximum baseline Z_N.

The values of N for a given α, for which the baseline Z_N is doubled, tripled and increased five times, are given by the intersections with the three dashed lines on the graph. For example, with a fractional bandwidth of $\alpha = .02$, the spatial frequency coverage is tripled if 80 baselines are used, and if $N = 100$ the maximum spatial frequency is five times greater than for the monochromatic case.

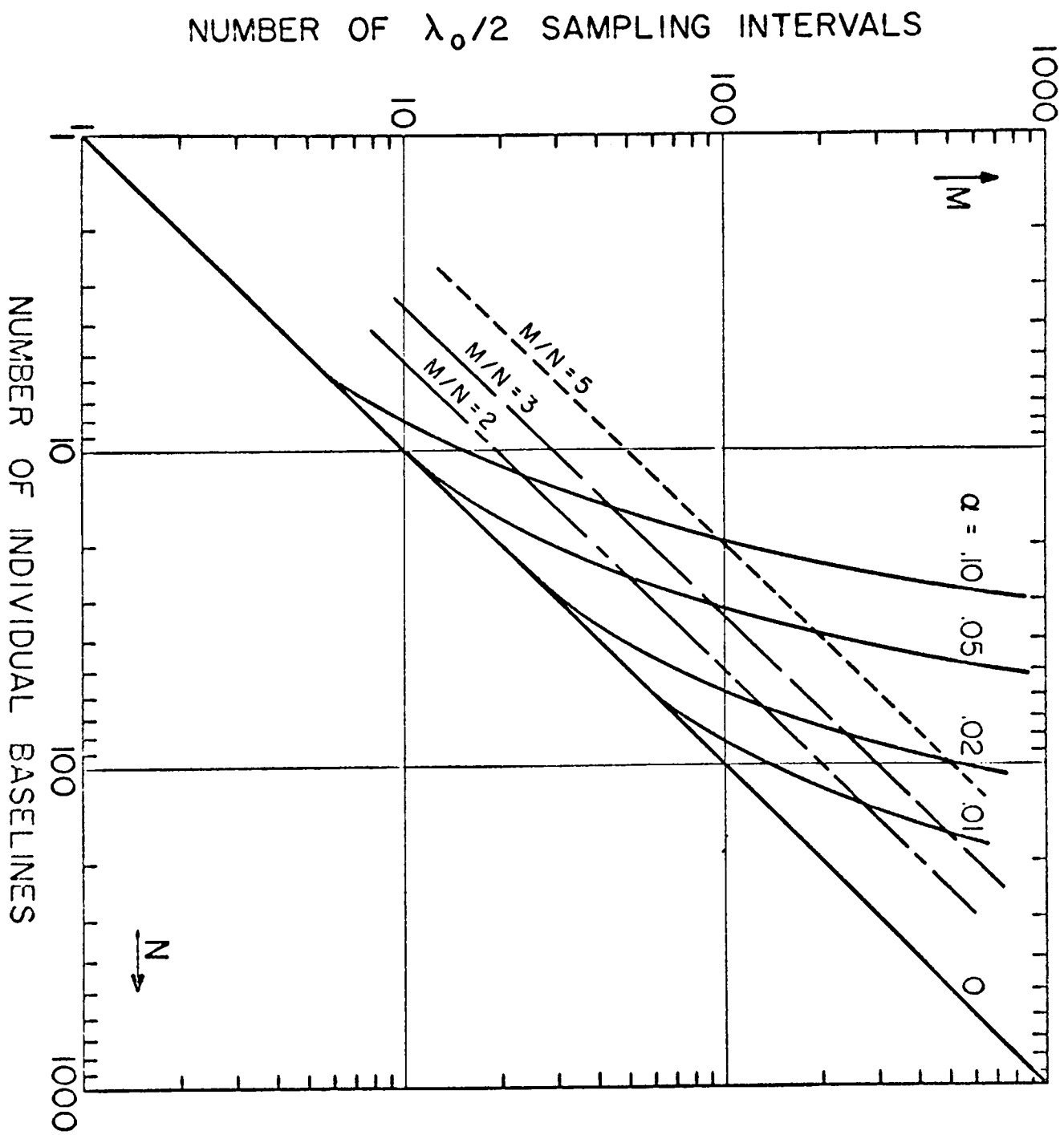

Figure 8: Number of $\frac{\lambda_0}{2}$ sampling intervals as a function of the number of baselines with the fractional bandwidth α as a parameter.

VI. MODIFICATION OF THE CORRELATION SYSTEM DUE TO THE BANDWIDTH

Let us consider a typical long baseline measurement by the two-element double-sideband interferometer, Again we assume that $\omega_1 = \pi B$. The spatial frequency passband is centered at

$$z_n = \left(\frac{1 + \alpha}{1 - \alpha}\right)^{(n - \bar{n})} \bar{n} \frac{\lambda_o}{2},$$

and its width is $2\alpha z_n$.

For the particular case of $\alpha = .02$ and $n = 65$, $z_n = 61.9\ \lambda_o$ and the bandwidth is $2.48\ \lambda_o$. Within this passband are five spatial frequency measurement points, viz., $61\ \lambda_o$, $61.5\ \lambda_o$, $62\ \lambda_o$, $62.5\ \lambda_o$, and $63\ \lambda_o$. The problem is to determine the spatial frequency spectrum at these points.

We begin by again considering the "bandwidth pattern" shown in Figure 3. Here the problem is to observe the sources outside the main lobe, sources for which $|u| > \frac{\omega_o}{2Bz_o}$. This can be easily done by <u>scanning</u> the bandwidth pattern by means of a time delay in the IF section of the correlator. Furthermore, since the bandwidth is B and the IF is $\omega_1 = \pi B$, the sampling theorem dictates that incremental delays of $\Delta\tau = \frac{1}{2B}$ will be sufficient to observe the entire source distribution.

In practice it is possible to have only a finite number of time delays. The appropriate number of delays can be easily deduced by considering the effect in the pattern domain where a delay $\Delta\tau$ corresponds to a shift of the beam of the equivalent monochromatic antenna by $\Delta u = \frac{\pi}{\alpha z_n}$. The number

of shifts must be sufficient to scan the beam over the entire visible range, for which $0 \leq \theta \leq \pi$ and $|u| \leq \frac{\omega_o}{c}$. Letting $Q\Delta u \simeq 2\frac{\omega_o}{c}$, we can obtain the number Q which will give a total scan slightly in excess of the full visible range,

$$Q = \left[\frac{2\omega_o}{c\Delta u}\right] = \left[4\alpha \frac{z_n}{\lambda_o}\right], \tag{16}$$

where [x] is the first integer greater than x. For the case of $\alpha = .02$ and $n = 65, Q = [4.95] = 5$; however, it will prove convenient to always let Q be an even number, and so in this case we let $Q = 6$. In general Q will be slightly larger than twice the spatial frequency passband, measured in wavelengths; this is a direct consequence of the sampling theorem.

Let us suppose that a point source is in the direction θ_o and we wish to measure its spatial frequency spectrum over the passband of the long-baseline interferometer. The output for a delay in the IF of $q\Delta\tau$ (accompanied by an RF phase delay of $qz_n\Delta u$) is

$$R'_{qn} = \frac{\sin[\alpha z_n (u_o - q\Delta u)]}{\alpha z_n (u_o - q\Delta u)} \cos[z_n(u_o - q\Delta u)]. \tag{17}$$

If we include the zero delay, we can obtain Q + 1 <u>real</u> outputs corresponding to a scan of the "bandwidth pattern" across the entire visible range $|u| \leq \frac{\omega_o}{c}$.

However, our task is to determine approximately Q complex spatial frequency components falling within the passband of the system. Clearly, we are missing half the information necessary to do this. The missing data can be easily obtained by the well-known technique of combining the element outputs in phase-quadrature. In the case of the point source at $u = u_o$, this gives the following outputs

$$R''_{qn} = \frac{\sin\,[\alpha z_n\,(u_o - q\Delta u)]}{\alpha z_n\,(u_o - q\Delta u)} \sin\,[z_n\,(u_o - q\Delta u)], \quad -\frac{Q}{2} \leq q \leq \frac{Q}{2}\,. \tag{18}$$

Then we define the complex output

$$R_{qn} = R'_{qn} + j\,R''_{qn}$$

$$= \frac{\sin\,[\alpha z_n\,(u_o - q\Delta u)]}{\alpha z_n\,(u_o - q\Delta u)}\; e^{j\,z_n\,(u_o - q\Delta u)}, \quad -\frac{Q}{2} \leq q \leq \frac{Q}{2}\,. \tag{19}$$

Now, as is well-known, a shift in the pattern by $q\Delta u$ corresponds to a multiplication of the spatial frequency spectrum by $e^{-jq\Delta uz}$ (the shifting theorem of Fourier analysis). Thus the spatial frequency spectrum corresponding to R_{qn} is

$$t_{qn}(z) = \frac{\pi}{\alpha z_n} R_{qn}\, e^{-jq\Delta uz}, \text{ for } \left|\,|z| - z_n\right| \leq \alpha z_n, \tag{20}$$

$$= 0 \quad \text{, otherwise.}$$

Letting $\bar{R}_{qn} = \frac{\pi}{\alpha z_n} R_{qn}$, we can expand the spatial frequency distribution as the following Fourier series:

$$t_n(z) = \sum_{q=-\frac{Q}{2}}^{\frac{Q}{2}} t_{qn}(z) = \sum_{q=-\frac{Q}{2}}^{\frac{Q}{2}} \bar{R}_{qn} e^{-jq\Delta uz}, \text{ for } \left| |z| - z_n \right| \leq \alpha z_n \quad (21)$$

$$= 0, \quad \text{otherwise.}$$

It can be shown that as Q increases without limit, $t_n(z)$ approaches the true distribution $t(z)$ in the mean square sense over the interval $\left| |z| - z_n \right| \leq \alpha z_n$. Now by setting $z = m \frac{\lambda_o}{2}$ in (21), with $\left| m \frac{\lambda_o}{2} - z_n \right| \leq \alpha z_n$, one obtains expressions for the spatial frequency distribution at the required half-wavelength intervals within the passband of the interferometer.

$$t_n(m \tfrac{\lambda_o}{2}) = t_{mn} = \sum_{q=-\frac{Q}{2}}^{\frac{Q}{2}} \bar{R}_{qn} e^{-jqm\frac{\Delta u \lambda_o}{2}} = \sum_{q=-\frac{Q}{2}}^{\frac{Q}{2}} \bar{R}_{qn} e_{qm}^{(n)}, \quad (22)$$

where $e_{qm}^{(n)} = \left(e^{-j\frac{\Delta u \lambda_o}{2}} \right)^{qm}$ can be thought of as the qm^{th} element of a rectangular matrix E_n.

Defining the column vectors T_n and $\bar{R}_n$ with elements t_{mn} and $\bar{R}_{qn}$, respectively, we can write the matrix equation

$$T_n = E_n \bar{R}_n \quad . \tag{23}$$

In practice $\bar{R}_n$ will have Q + 1 elements and T_n will have Q or Q -1 elements. Consequently, E_n will not be a square matrix. Equations (23) defines the way in which the complex interferometer output vector $\bar{R}_n$ is transformed into the required complex spatial frequency vector T_n. This operation should be very easy to perform with a digital computer.

For the case of $\alpha = .02$, $n = 65$ and a point source at $\theta_o = 45°$, the elements of the vectors $\bar{R}_{65}$ and T_{65} are given in Table 1, for several values of Q. For comparison, the exact value of T_{65} is also given. The validity of truncating the time delays to a finite number, in this case to $Q = 6$, is illustrated in Figure 9 where the exact and approximate values of $t_{m\ 65}$ are plotted.

In general we can use (16) to deduce a relation between Q, α, and $N_{\alpha Q}$, where the $n = N_{\alpha Q}{}^{th}$ baseline is the last for which only Q time delays are required when the bandwidth is α. These numbers for a variety of α's and Q's are given in Table 2. For example, if $\alpha = .02$, the first 25 baselines are at the usual increments of $\frac{\lambda_o}{2}$. The next 17 baselines, up to the 43rd, will be shifted according to equation (13) and the two time delays will be necessary for each baseline (as well as the usual zero delay). From the 44th to the 60th baseline, four time delays will be necessary; from the 61st to the 70th, six delays must be used, and so on.

VII. TWO DIMENSIONAL INTERFEROMETRY -- THE U-V PLANE

We now consider the important practical case of interferometry in two dimensions where the baselines are located in a plane--the u-v plane.

$\bar{R}_{65}$ - DATA VECTORS - $\bar{R}_{65}$								
	Real Part				Imaginary Part			
Q / q	4	6	8		4	6	8	
-4			-.00938				-.03816	
-3		.01136	.01136			.04620	.04620	
-2	-.01436	-.01436	-.01436		-.05851	-.05851	-.05851	
-1	.01962	.01962	.01962		.07978	.07978	.07978	
0	-.03082	-.03082	-.03082		-.12533	-.12533	-.12533	
1	.07183	.07183	.07183		.29210	.29210	.29210	
2	.21727	.21727	.21727		.88352	.88352	.88352	
3		-.04324	-.04324			-.17583	-.17583	
4			.02401				.09763	

T_{65} - SOLUTION VECTORS - T_{65}								
	Real Part				Imaginary Part			
Q / m	4	6	8	Exact	4	6	8	Exact
122	.6929	.8235	.8051	.6683	.5925	.7239	.7823	.7438
123	-1.0704	-1.0611	-.9410	-.9967	-.1715	-.0370	-.0905	-.0811
124	.6323	.4869	.5902	.5393	-.9132	-.8326	-.8534	-.8422
125	.2080	.4277	.3805	.3436	.9906	.9981	.9300	.9397
126	-.5906	-.7916	-.9281	-.9553	-.2389	-.3313	-.3586	-.2954

Table 1. Data and solution vectors for the case of $\alpha = .02$, $n = 65$, and unit point source at $\theta_o = \pi/4$.

$N_{\alpha Q}$						
α \ Q	0	2	4	6	8	10
.10	5	9	12	14	16	17
.05	10	17	24	28	31	33
.02	25	43	60	70	78	83
.01	50	85	120	140	155	167

THE $N_{\alpha Q}$ th INTERFEROMETER BASELINE IS THE LAST BASELINE FOR WHICH Q TIME DELAYS ARE REQUIRED WITH A RELATIVE BANDWIDTH OF α.

Table 2: Relation between the $N_{\alpha Q}^{th}$ baseline, the bandwidth α, and the required number of time delays Q.

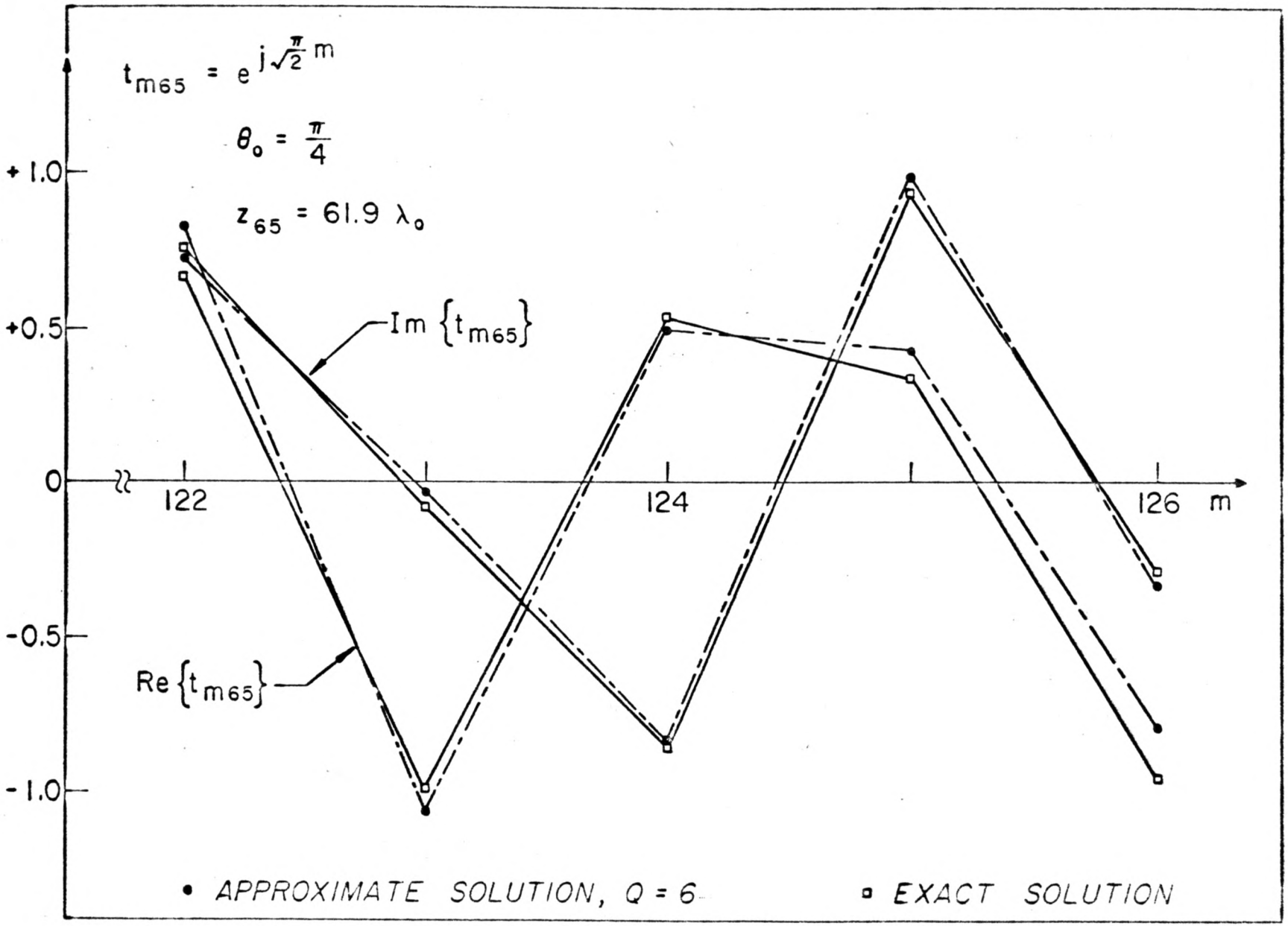

Figure 9: Spatial frequency spectra for the case of a point source at $\theta_0 = \frac{\pi}{4}$ and an interferometer baseline of $61.9\lambda_0$, fractional bandwidth $\alpha = 0.02$.

The effect of bandwidth on the spatial frequency response of a broadband interferometer whose baseline of length ρ_o is oriented at the angle σ_o to the east-west direction (the u-axis) is shown in Figure 10. The spatial frequency passband (when $\omega_1 = \pi B$, with double-sideband operation) is of length $2\alpha\rho_o$ along the radial baseline, with the mid-point of the passband located at the position (ρ_o, σ_o). The spatial frequency "smearing" due to bandwidth is in the radial direction; there is no tangential dispersion.

Now as in the one-dimensional case, for long baselines the radial passband may extend over many half wavelengths, thus permitting an increase in the spacing of the long baselines. Indeed the formula relating the radial baselines in the u-v plane is identical to that for the linear one-dimensional case.

The circles in the u-v plane on which baselines should be located are centered at the origin and are of radius

$$\rho_n = n \frac{\lambda_o}{2} \quad , \quad \text{for } n \leq \bar{n} \quad , \tag{24}$$

$$\rho_n = \left(\frac{1+\alpha}{1-\alpha}\right)^{n-\bar{n}} \bar{n} \frac{\lambda_o}{2} \quad , \quad \text{for } n > \bar{n} \quad , \tag{25}$$

where $\bar{n} = \left[\frac{1-\alpha}{2\alpha}\right]$.

In the above, we assume double sideband operation with $\omega_1 = \pi B$ and $\alpha = \frac{2\pi B}{\omega_o}$.

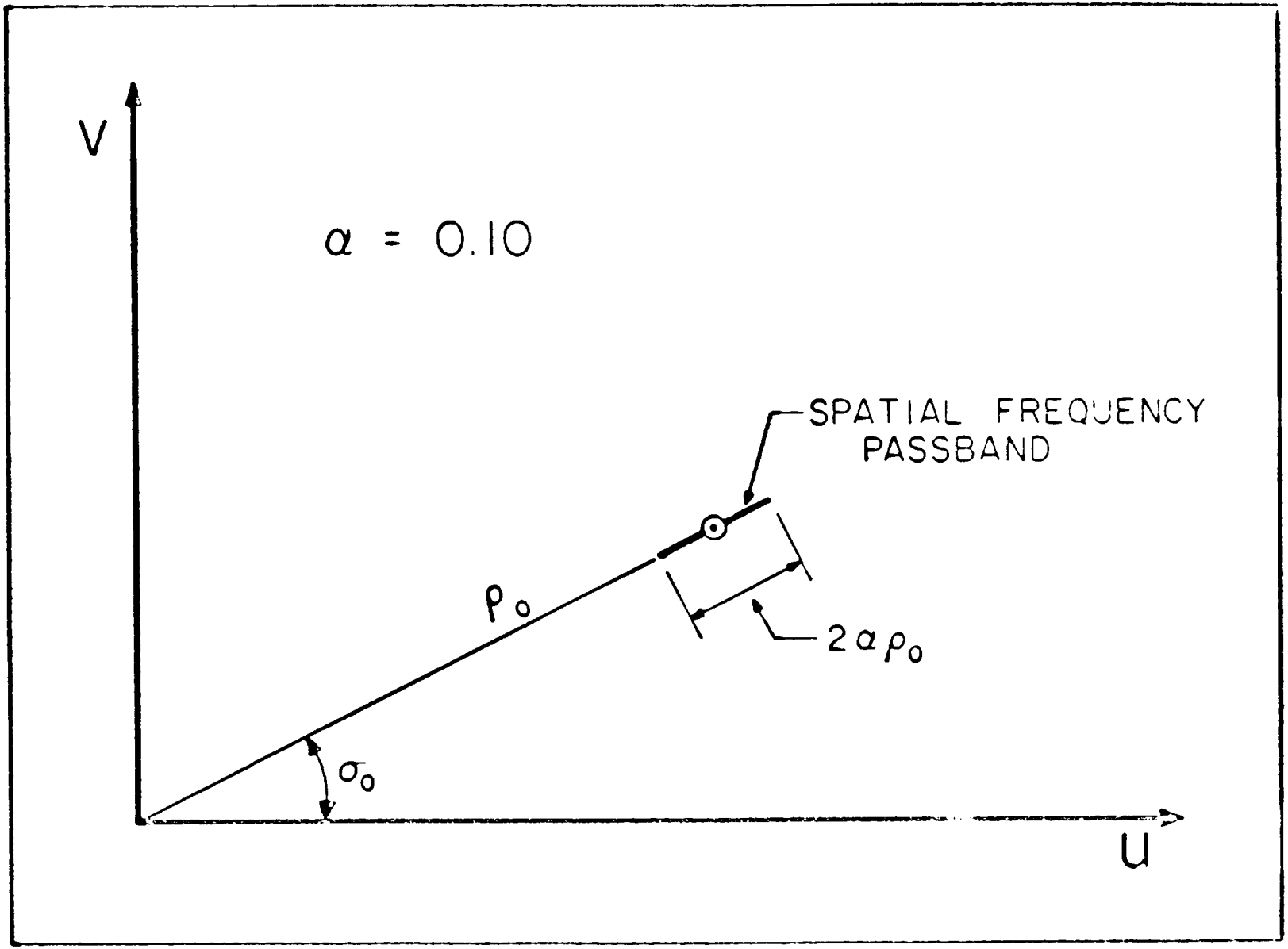

Figure 10: Spatial frequency passband in the u - v plane for a broadband interferometer with baseline of length ρ_0.

In the circumferential direction there must be a density of two baselines per wavelength. Consequently, on the n^{th} baseline circle the angular separation between baselines is $\Delta\sigma_n = \frac{\lambda_o}{2\rho_n}$, and if we consider only a half circle in the u-v plane (the spatial frequency spectrum is symmetric) the number of baselines on the half circle is

$$b_n = \left[\frac{\pi}{\Delta\sigma_n}\right] = \left[\frac{\omega_o}{c}\ \rho_n\right] = \left[2\pi\ \frac{\rho_n}{\lambda_o}\right]. \tag{26}$$

In Figure 11 are shown the baselines in the first quadrant of the u-v plane for the case when $\alpha = 0.1$.

Finally, it can be shown that for $\bar{N}$ circles, the total number of baselines is

$$N = \pi\bar{n}\left\{\frac{\bar{n}+1}{2} + \frac{1+\alpha}{2\alpha}\left[\left(\frac{1+\alpha}{1-\alpha}\right)^{\bar{N}-\bar{n}} - 1\right]\right\} \tag{27}$$

and that the number of sample points spaced $\frac{\lambda_o}{2}$ apart, four points per square wavelength, which lie within the passbands of the $\bar{N}$ circles, is

$$M = \frac{\pi}{2}\ [(1+\alpha)\ \bar{n}]^2\ \left(\frac{1+\alpha}{1-\alpha}\right)^{2\ (\bar{N}-\bar{n})}. \tag{28}$$

The graph of M vs. N, for various values of α, is shown in Figure 12. This is analogous to the one-dimensional interferometer graph given in Figure 8.

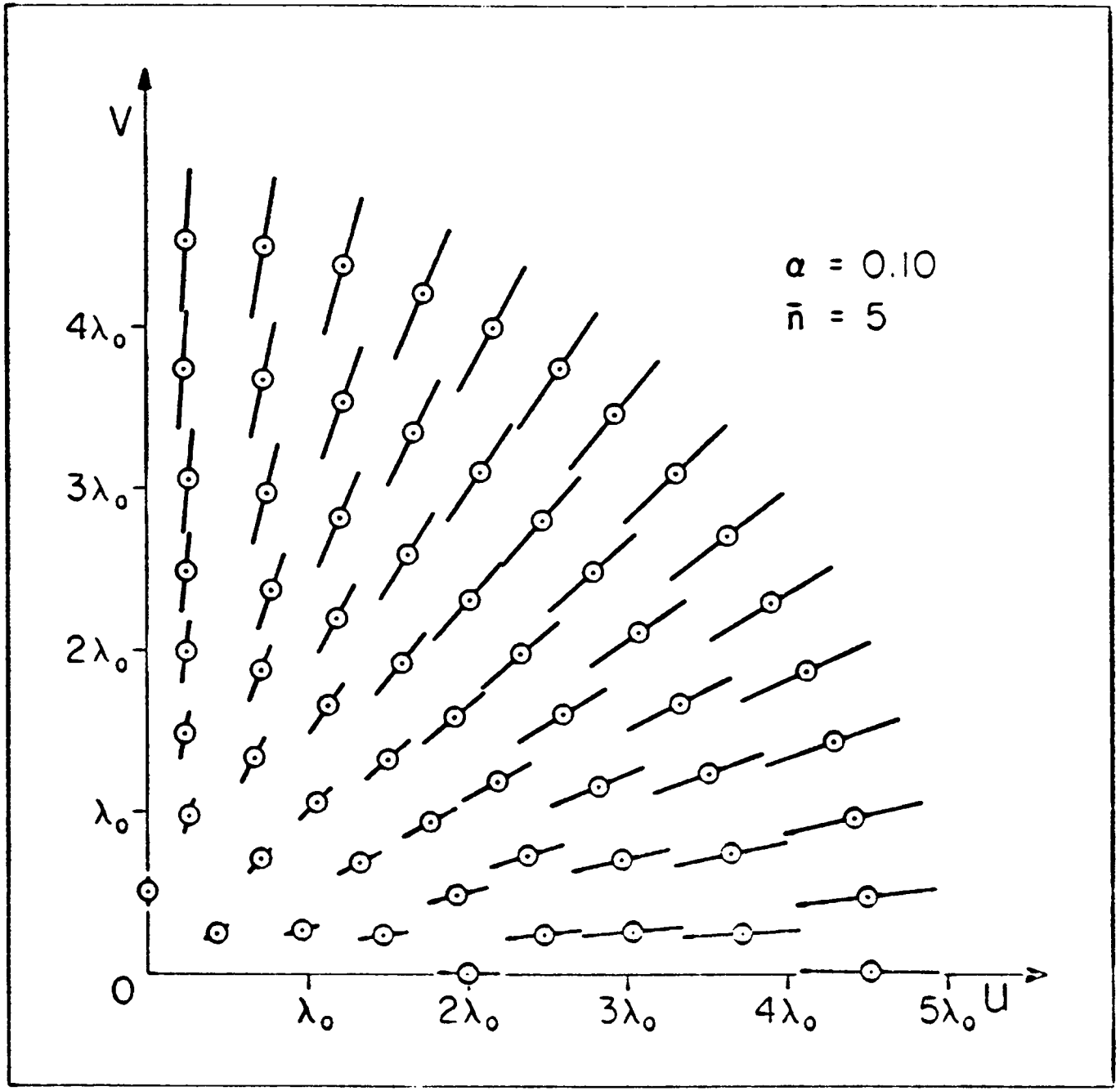

Figure 11: Spatial frequency distribution in u - v plane showing sampling locations and dispersion of long-baseline passbands.

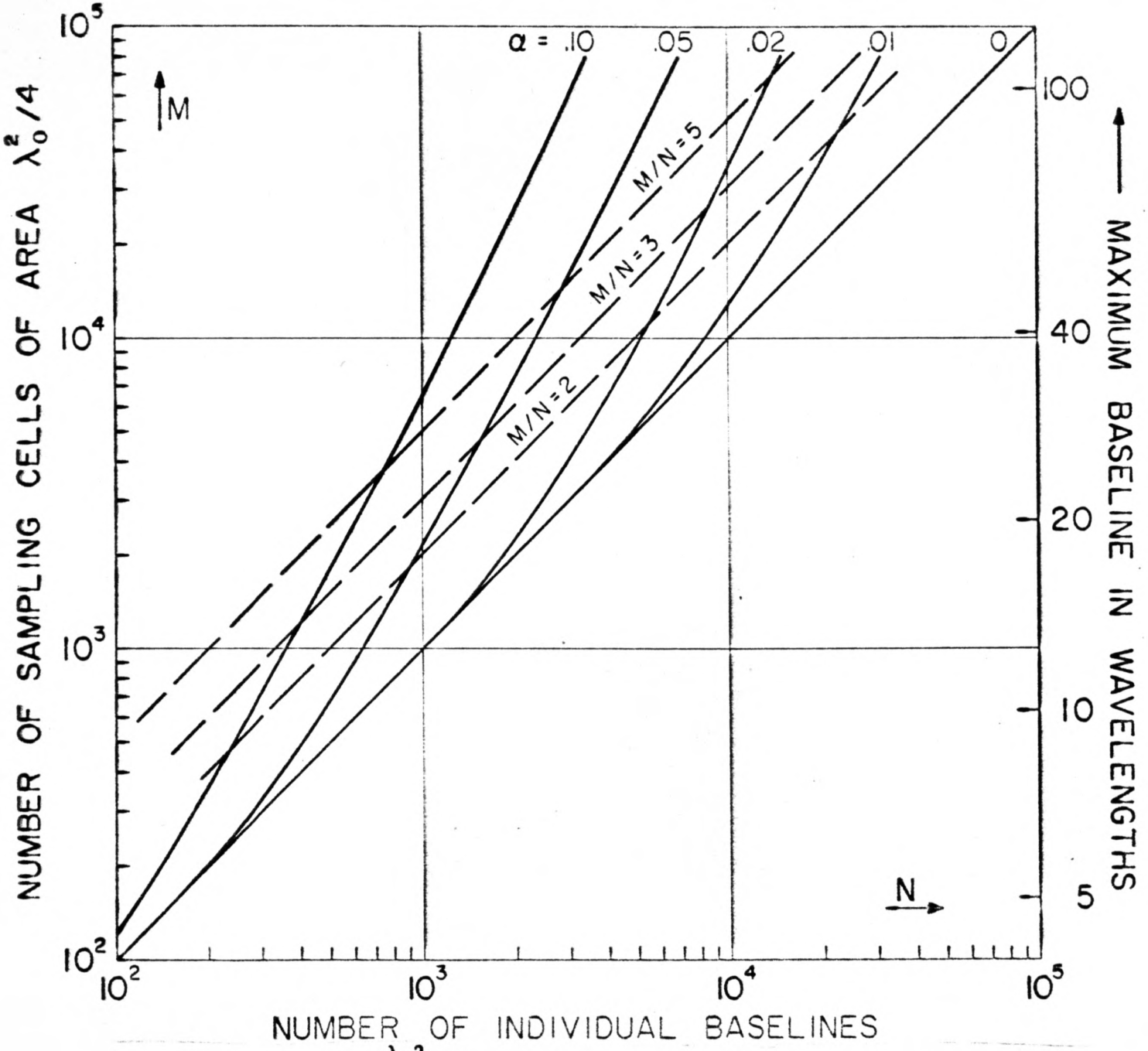

Figure 12: Number of $\frac{\lambda_0^2}{4}$ sampling cells as a function of the number of baselines in the u - v plane with the fractional bandwidth α as a parameter.

VIII. SIGNAL PROCESSING IN THE TWO-DIMENSIONAL CASE

At long baselines $Q + 1$ outputs are obtained from the interferometer, where for double-sideband operation, with $\omega_1 = \pi B$, $Q = \left\lfloor 4\,\alpha\,\frac{\rho_n}{\lambda_o} \right\rfloor$. The outputs are obtained by incrementally changing the correlator time delay by $q\Delta\tau$ seconds, with $-\frac{Q}{2} \le q \le \frac{Q}{2}$, and $\Delta\tau = \frac{1}{2B}$.

For a point source in the direction* (x_o, y_o) and for a baseline with coordinates $(u_{nm}, v_{nm}) = (\rho_n, \sigma_{nm})$ the output for the q^{th} delay is

$$R_{qnm} = \frac{\sin\left[\alpha\left(u_{nm}x_o + v_{nm}y_o\right) - q\pi\right]}{\alpha\left(u_{nm}x_o + v_{nm}y_o\right) - q\pi}\; e^{j\left[u_{nm}x_o + v_{nm}y_o - \frac{q\pi}{\alpha}\right]}. \qquad (29)$$

The position angle σ_{nm} indicates the angle of the m^{th} baseline $(1 \le m \le b_n)$ on the n^{th} circle of radius ρ_n. Equation (29) is the two-dimensional analog of (19). In Appendix B it is shown that the analog of (20), in the two-dimensional spatial frequency plane, is

$$\begin{aligned} t_{qnm}(u,v) &= \bar{t}_{qnm}(\rho,\sigma) \\ &= R_{qnm}\,(2\pi)^2\,\frac{\delta(\sigma - \sigma_{nm})}{2\,\alpha\rho_n\rho}\; e^{-jq\pi\frac{\rho}{\alpha\rho_n}}, \text{ for } |\rho - \rho_n| \le \alpha\rho_n \qquad (30) \\ &= 0, \text{ otherwise.} \end{aligned}$$

---

* If θ is the angle measured from the normal to the u-v plane and ϕ the azimuth angle measured from the u-axis, then for an operating frequency ω_o we have $x = \frac{\omega_o}{c}\sin\theta\cos\phi$, $y = \frac{\omega_o}{c}\sin\theta\sin\phi$; if u and v are measured in meters, then ux + vy is in radians.

The series expansion for the spectrum is

$$\bar{t}_{nm}(\rho,\sigma) = \sum_{q=-\frac{Q}{2}}^{\frac{Q}{2}} \bar{t}_{qnm}(\rho,\sigma) \tag{31}$$

from which the spatial frequency coefficients at intervals of $\frac{\lambda_o}{2}$ in the radial direction may be obtained. The analog of (22) is

$$\bar{t}_{nmr} = \frac{(2\pi)^2}{r\alpha\lambda_o\rho_n} \sum_{q=-\frac{Q}{2}}^{\frac{Q}{2}} R_{qnm}\, e^{(n)}_{qmr}, \quad \text{for } \sigma = \sigma_{nm}, \tag{32}$$

where

$$e^{(n)}_{qmr} = \left(e^{-j\frac{\pi\lambda_o}{2\alpha\rho_n}}\right)^{qr}, \quad \text{and} \quad (1-\alpha)\,\rho_n \le r\frac{\lambda_o}{2} \le (1+\alpha)\,\rho_n.$$

The complex number $\bar{t}_{nmr}$ is the spatial frequency component at the point $\left(r\frac{\lambda_o}{2}, \sigma_{nm}\right) = \left(u_{nmr}, v_{nmr}\right)$ in the u-v plane. The brightness temperature map is finally synthesized by using the M components in the following Fourier series.

$$T(x,y) = \sum_{n=1}^{\bar{N}} \sum_{m=1}^{b_n} \sum_{r=1}^{Q} \bar{t}_{mnr}\, e^{-j(u_{nmr}x + v_{nmr}y)} \tag{33}$$

where, as in the one-dimensional case, $Q = \left[4\alpha\frac{\rho_n}{\lambda_o}\right]$.

IX. ON THE USE OF LARGE DISHES AS ELEMENTS

In practice, the elements of long baseline interferometers are usually highly directive large parabolic dishes, as is the case in the VLA Proposal [5]. Then the system output, for one-dimensional patterns, becomes

$$P(u) = P_e(u_o - u) \left\{ \frac{\sin\left[\frac{\pi B}{\omega_o} z_o(u_o - u)\right]}{\frac{\pi B}{\omega_o} z_o(u_o - u)} \cos\left[\frac{\omega_1}{\omega} z_o(u_o - u)\right] \right\} e^{jz_o(u_o - u)} \qquad (34)$$

where $P_e(u)$ is the power pattern of the elements which are assumed to be identical.

In the spatial frequency domain, the actual spectrum is the convolution of the isotropic spectrum as given by (5) and Figure 4, with the spectrum of the elements, $p_e(z)$. For example, if the elements are uniformly illuminated over the aperture D, then the element spectrum is triangular in shape as is shown in Figure 13(a). In Figures 13(b) and 13(c) are shown the spatial frequency spectra of the interferometer (in double sideband operation with $\omega_1 = \pi B$) for short and long baselines, respectively. Clearly the interferometer baseline intervals, which for short baselines must be equal to 2D, can be <u>exponentially increased</u> as the baseline lengthens. With regard to the triangular taper towards the edges of the elements' spatial frequency passband, it is possible with a correlation system to illuminate the apertures of the elements with an <u>inverse taper</u> and obtain a rectangular element spectrum [8].

The effect of element size and bandwidth on the pattern is illustrated in Figure 14. At short baselines the element pattern limits the field of view to $2\Delta u_g = 2\left(\frac{2.78}{D}\right)$ between half-power points. At long baselines the

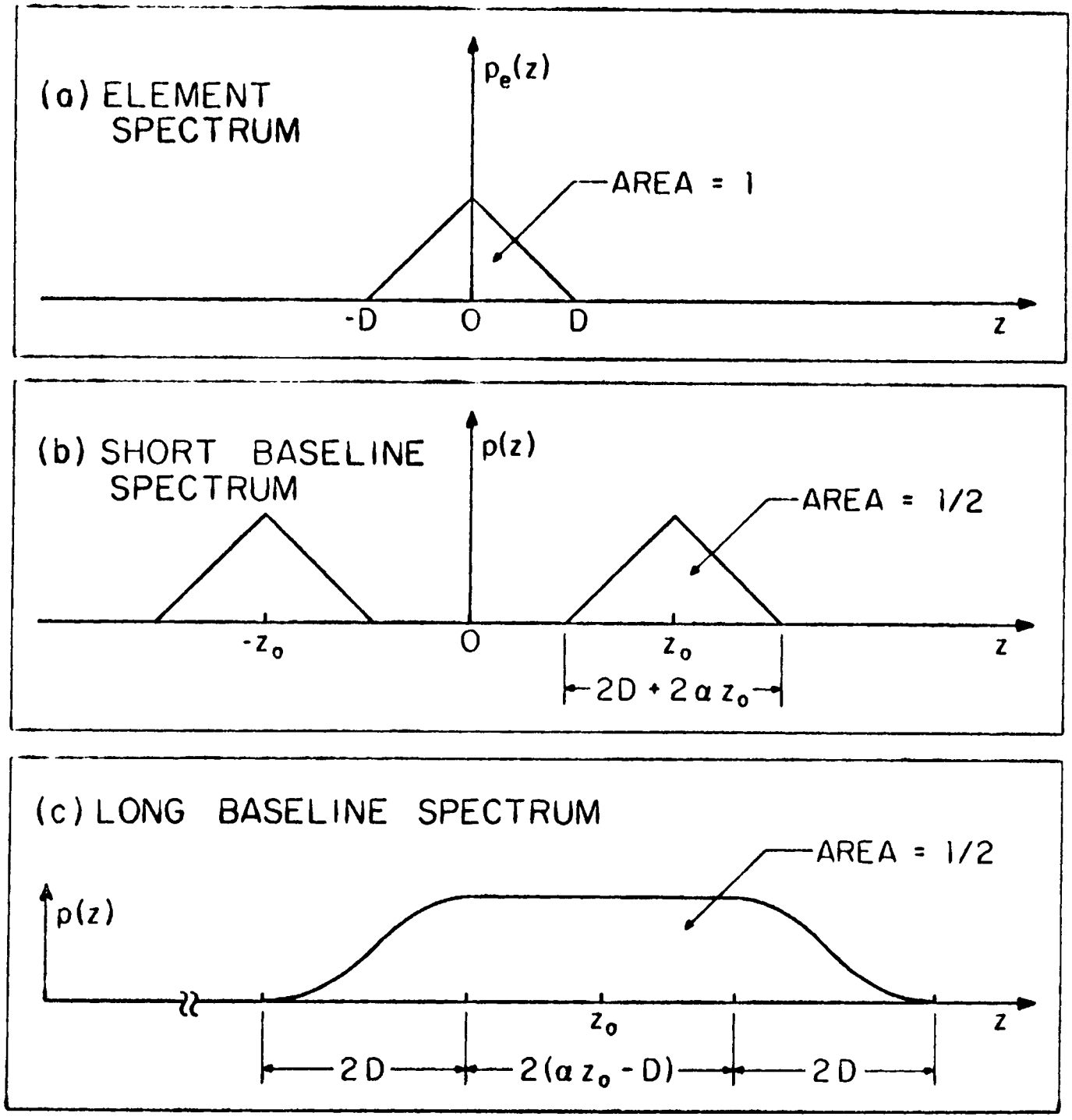

Figure 13: Spatial frequency spectra for an interferometer using elements of diameter D.

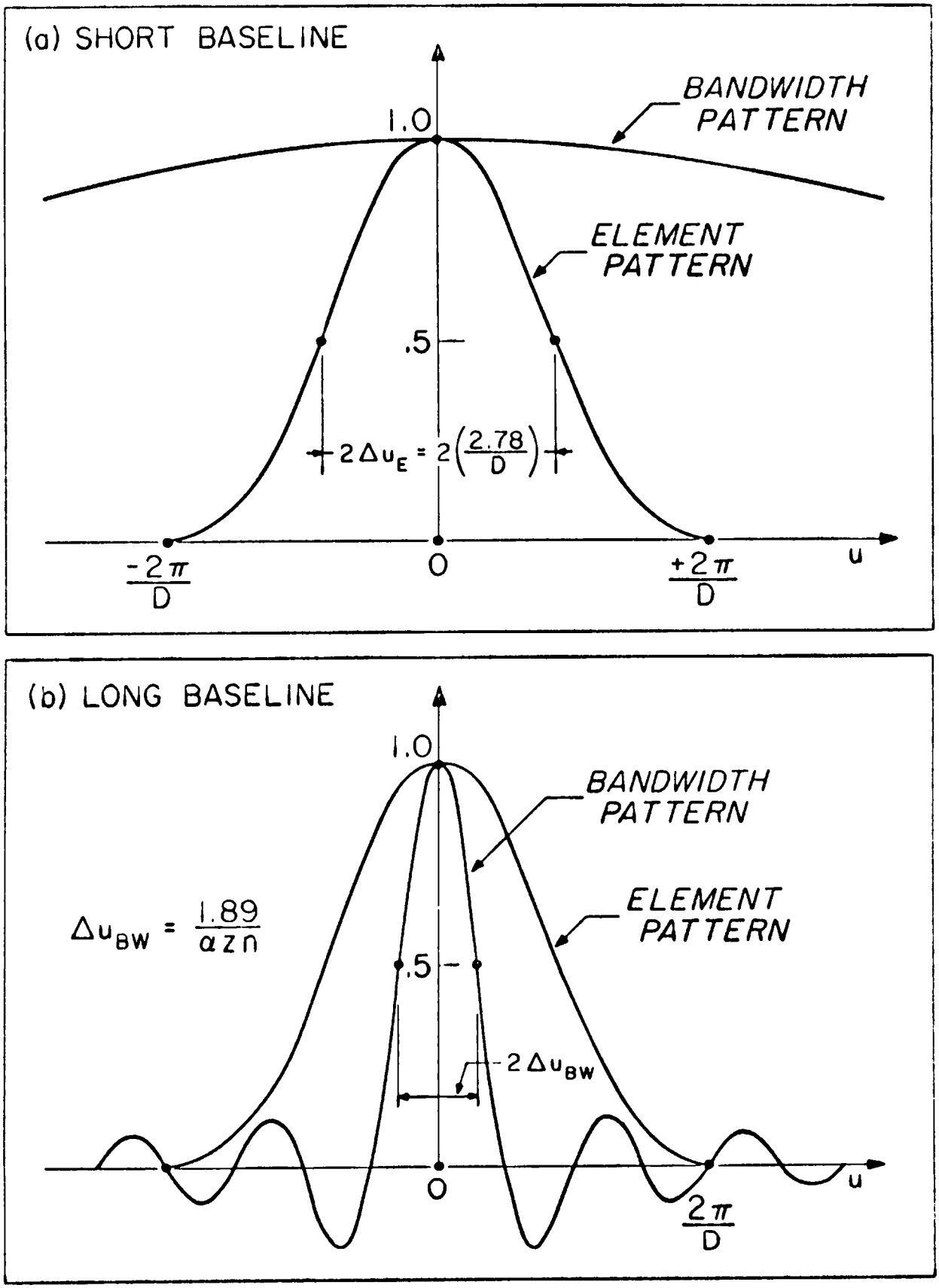

Figure 14: Relation of element and bandwidth patterns for short and long baselines.

limitation is primarily due to the bandwidth pattern whose field of view between half-power points is $2\Delta u_{BW} = 2(\frac{1.89}{\alpha z_n})$.

X. SOME REMARKS ON NOISE

Witnessing the reduction in magnitude of the spatial frequency spectrum with increasing baselines (see the staircase characteristic of Figure 7), one might expect a corresponding decrease in the signal-to-noise ratio of the interferometer outputs, r_{mn}. However, unlike the short baseline interferometers for which it is sufficient to make a single measurement, with an integration time of say T seconds, in the long baseline case there are Q + 1 measurements, each of duration T seconds*. From these Q + 1 measurements $\bar{R}_{qn}$, one can use the matrix equation (23) to determine the Q spatial frequency components t_{mn}. Consequently the integration time per spatial frequency component is approximately the same for all components. There should be no degradation in the accuracy with which the long baseline components are measured.

XI. CONCLUSIONS

As a result of the non-zero bandwidth of any practical radio interferometer, a "bandwidth pattern" arises as a factor in the interferometer output, a pattern whose directivity is proportional to the product of the bandwidth and the length of the baseline. The narrowing of the field of view due to the "bandwidth pattern" can be overcome by scanning the pattern with time delays in the IF of the interferometer receiver.

In the spatial frequency domain the effect is to produce passbands centered at the nominal baseline of the interferometer and of width proportional to the baseline-bandwidth product. For long baselines the spatial

---

* Alternatively, by power dividing the signals into Q + 1 parts one can use Q + 1 correlators, each with a different time delay, and each with an averag- time of (Q + 1) T seconds to obtain simultaneously the Q + 1 measurements.

frequency passbands extend over many sample points used in conventional aperture synthesis. The receiver time delays produce a series of independent outputs from the fixed-baseline interferometer and by a simple Fourier matrix transformation of this data, one can deduce the required spatial frequency components lying within the interferometer's passband. Consequently, a complete aperture synthesis can be achieved by using a reduced number of individual baselines. Indeed, the sampling interval may be increased exponentially as the baseline lengthens yielding, for large aperture synthesis, an exponential reduction in the number of baselines.

It is interesting to note that the interferometer spacings, as proposed here, are logarithmically periodic, and hence the geometry coincides with that of the broadband log-periodic structures developed at the University of Illinois. However, the present system uses a single broadband signal centered at a specific frequency, whereas log-periodic structures use a number of independent narrow-band signals discretely spaced over a broadband of frequencies. Thus the structural similarity is purely coincidental.

Finally, the recent Canadian success with the very long baseline interferometer between Penticton, British Columbia, and Algonquin Park, Ontario, a baseline of several million wavelengths, leads one to estimate the saving in baseline positions for, say, a synthesized aperture of one million wavelengths with interferometer dishes with diameters of 250 wavelengths. For complete aperture synthesis 2,000 sample points are required. However, with a double-sideband interferometer with a one percent bandwidth only 270 individual baselines are needed, and for a five percent bandwidth 70 baselines are sufficient. The resolution of the synthesized pattern (Rayleigh criterion) would be 1/10 of a second of arc.

ACKNOWLEDGEMENT

The author would like to express thanks to Dr. G. W. Swenson, Jr., for his invitation to visit NRAO, to Dr. E. J. Blum for his many helpful comments, to Dr. Peter Stumpff and Mr. Neil Stoltzfus for their help with the computations, and to Dr. H. M. Hrabikova, Georgetown University, for inspiration.

REFERENCES

1. W. E. Koch and J. L. Stone, "Space-frequency equivalence," Proc. IRE, vol. 46, No. 2, pp. 499-500, February 1958.

2. M. Ryle, "A new radio interferometer and its application to the observation of weak radio stars," Proc. Roy. Soc. London,Ser. A, vol. 211, pp. 351-375, 1952.

3. R. N. Bracewell, "Radio interferometry of discrete sources," Proc. IRE, vol. 46, No. 1, pp. 97-105, January 1958.

4. M. Ryle, A. Hewish and J. R. Shakeshaft, "The synthesis of large radio telescopes by the use of radio interferometers," IRE Trans. on Antennas and Propagation, vol. AP-7, suppl., pp. S120-124, December 1959.

5. "The VLA--a proposal for a very large array radio telescope," Report of the National Radio Astronomy Observatory, Green Bank, West Virginia, U.S.A., January 1967.

6. R. N. Bracewell and J. A. Roberts, "Aerial smoothing in radio astronomy," Australian J. Phys. vol. 7, pp. 615, 640, December 1954.

7. R. B. Read, "Accurate measurement of the declinations of radio sources," Astrophysical Journal, vol. 138, No. 1, pp. 1-29, July 1963.

8. R.R.N. Utukuri and R. H. MacPhie, "Coincident arrays for the direct measurement of the principal solution in radio astronomy," IEEE Trans. PGAP, vol. AP-15, No. 1, pp. 49-59, January 1967.

APPENDIX A

Analysis of the Output of a Double Sideband Correlation Interferometer

With reference to Figure 1, the output is the cross correlation of two complex signals $W_1(t)$ and $W_2(t)$.

$$R(\tau) = \langle W_1(t)\, W_2^*(t-\tau) \rangle$$

$$= \langle [\mathrm{Re}\,\{V(t)\} \ast f(t)]\, [\mathrm{Re}\,\{V(t + \tau_o - \tau)\, e^{j\gamma}\} \ast f^*(t-\tau)] \rangle$$

where * indicates the complex conjugate, Re {...} indicates "the real part of ...", and f(t) is the impulse response of the IF filters. V(t) is the modulation envelope of the signal, a complex gaussian random process.

Written out in terms of integrals, we have

$$R(\tau) = \lim_{T\to\infty} \frac{1}{2T} \int_{-T}^{T} \int_{-\infty}^{\infty} \mathrm{Re}\,\{V(t - t_1)\}\ f(t_1)\, dt_1 \int_{-\infty}^{\infty} \mathrm{Re}\,\{V(\tau_o - \tau + t - t_2) e^{j\gamma}\}$$

$$f^*(t_2)\, dt_2\, dt.$$

Interchanging the order of integration, we obtain

$$R(\tau) = \int_{-\infty}^{\infty} \int_{-\infty}^{\infty} f(t_1)\ f^*(t_2)\ \lim_{T\to\infty} \frac{1}{2T} \int_{-T}^{T} \mathrm{Re}\,\{V(t - t_1)\}$$

$$\mathrm{Re}\,\{V(\tau_o - \tau + t - t_2)\, e^{j\gamma}\}\, dt\, dt_1\, dt_2.$$

It is easy to show that the integral on t becomes

$$\frac{1}{2}\,\mathrm{Re}\,\{\lim_{T\to\infty}\frac{1}{2T}\int_{-T}^{T} V(t-t_1)\,V^{*}(\tau-\tau_o+t-t_2)\,e^{-j\gamma}\,dt\} =$$

$$= \frac{1}{2}\,\mathrm{Re}\,\{R_{VV}\,[\tau-\tau_o-(t_1-t_2)]\,e^{-j\gamma}\}$$

where $R_{VV}(\tau)$ is the autocorrelation function of $V(t)$. Then if we define $t_3 = t_1 - t_2$, we get

$$R(\tau) = \frac{1}{2}\int_{-\infty}^{\infty}\int_{-\infty}^{\infty} f(t_1)\,f^{*}(t_1-t_3)\,\mathrm{Re}\,\{R_{VV}\,(\tau-\tau_o-t_3)\,e^{-j\gamma}\}dt_1\,dt_3$$

$$= \frac{1}{2}\int_{\infty}^{\infty}\left[\int_{-\infty}^{\infty} f(t_1)\,f^{*}\,(t_1-t_3)\,dt_1\right]\mathrm{Re}\,\{R_{VV}\,(\tau-\tau_o-t_3)\,e^{-j\gamma}\}dt_3$$

$$= \frac{1}{2}\int_{-\infty}^{\infty} R_{ff}\,(t_3)\,\mathrm{Re}\,\{R_{VV}\,(\tau-\tau_o-\tau_3)\,e^{-j\gamma}\}\,dt_3$$

$$R(\tau) = \frac{1}{2}\,R_{ff}\,(\tau-\tau_o) \ast \mathrm{Re}\,\{R_{VV}\,(\tau-\tau_o)\,e^{-j\gamma}\}$$

Now by the convolution and shifting theorems, we have the following power spectra relation

$$R(\omega) = \frac{1}{4}\,r_{ff}\,(\omega)\,\{r_{VV}\,(\omega)\,e^{-j\gamma} + r^{*}_{VV}\,(\omega)\,e^{j\gamma}\}\,e^{j\omega\tau_o}.$$

If we assume that both $r_{ff}(\omega)$ and $r_{VV}(\omega)$ are white noise spectra with

$$r_{ff}(\omega) = 1, \quad \text{for } |\omega-\omega_1| \leq \pi B$$
$$= 0, \quad \text{otherwise}$$

and $$r_{VV}(\omega) = S, \quad \text{for } |\omega| < \omega_2 >> \omega_1$$

then we can write

$$r(\omega) = 1/2\ S \cos\gamma e^{j\omega\tau_o}, \text{ for } |\omega-\omega_1| \leq \pi B$$
$$= 0, \text{ otherwise.}$$

Taking the inverse transform of $r(\omega)$, we get

$$R(\tau) = \frac{S \cos\gamma}{2} \int_{\omega_1 - \pi B}^{\omega_1 + \pi B} e^{j\omega(\tau_o-\tau)}\, d\omega$$

$$= S\pi B \cos\gamma\ \frac{\sin[\pi B(\tau_o-\tau)}{\pi B(\tau_o-\tau)}\ e^{j\omega_1(\tau_o-\tau)}.$$

Taking the real part, we obtain

$$R'(\tau) = S\pi B \left\{\frac{\sin[\pi B(\tau_o-\tau)]}{\pi B(\tau_o-\tau)} \cos[\omega_1(\tau_o-\tau)]\right\} \cos[\omega_o \tau_o - \phi]$$

Except for the constant factor $S\pi B$, this is equal to $R'(\tau)$ as given by Equation (1), with $\tau_o = 0$ and $\phi = \omega_o\tau$.

APPENDIX B

Spatial Frequency Spectrum in the U-V Plane of the Broadband Interferometer

Since the spectrum is dispersed in the radial direction it is convenient to use polar coordinates. We let $u = \rho \cos \sigma$, $v = \rho \sin \sigma$ and consider the distribution

$$p(u,v) = \bar{p}(\rho,\sigma) = (2\pi)^2 \frac{\delta(\sigma - \sigma_o)}{2\alpha\rho_o\rho}, \text{ for } |\rho - \rho_o| \leq \alpha\rho_o$$

$$= 0, \text{ otherwise,}$$

where $\delta(\sigma)$ is the Dirac delta. The distribution is shown graphically in Figure 10. The Fourier transform is

$$P(x,y) = \mathcal{F}\{p(u,v)\} = \frac{1}{4\pi^2} \int\int p(u,v) e^{-j(ux + vy)} du dv.$$

Converting to polar coordinates we obtain

$$P(x,y) = \int_{\rho_o(1-\alpha)}^{\rho_o(1+\alpha)} \int_o^{2\pi} \frac{\delta(\sigma - \sigma_o)}{2\alpha\rho_o\rho} e^{-j(ux + uy)} \rho d\rho d\sigma$$

Now if we regard (x,y) and (u,v) as the vectors $\vec{Z}$ and $\vec{\rho}$ respectively, with $x = Z\cos\zeta$, $y = Z\sin\zeta$, $u = \rho\cos\sigma$, $v = \rho\sin\sigma$, then it is easy to show that $ux + vy = \vec{Z} \cdot \vec{\rho} = Z\rho\cos(\zeta - \sigma)$.

Then the Fourier transform can be written as

$$p(x,y) = \int_{\rho_o(1+\alpha)}^{\rho_o(1+\alpha)} \int_o^{2\pi} \frac{\delta(\sigma - \sigma_o)}{2\alpha\rho_o} e^{-jZ\rho\cos(\zeta - \sigma)} d\rho d\sigma$$

$$= \frac{1}{2\alpha\rho_o} \int_{\rho_o(1-\alpha)}^{\rho_o(1+\alpha)} e^{-jZ\cos(\zeta - \sigma_o)\rho}\, d\rho$$

$$= \frac{\sin[\alpha\rho_o Z\cos(\zeta-\sigma_o)]}{\alpha\rho_o Z\cos(\zeta-\sigma_o)}\, e^{-j\rho_o Z\cos(\zeta-\sigma_o)}$$

$$= \frac{\sin[\alpha(u_o x + v_o y)]}{\alpha(u_o x + v_o y)}\, e^{-j(u_o x + v_o y)}$$

which is the interferometer output for double sideband operation with $w_1 = \pi B$.

Now if we change the spectrum to

$$\bar{p}(\rho,\sigma) = (2\pi)^2 \frac{\delta(\sigma-\sigma_o)}{2\alpha\rho_o\rho}\, e^{jq\pi\frac{\rho}{\alpha\rho_o}}, \text{ for } |\rho-\rho_o| \le \alpha\rho_o,$$

$$= 0, \text{ otherwise,}$$

the Fourier transform becomes

$$P(x,y) = \frac{1}{2\alpha\rho_o} \int_{\rho_o(1-\alpha)}^{\rho_o(1+\alpha)} e^{-j[Z\cos(\zeta-\zeta_o) - \frac{q\pi}{\alpha\rho_o}]\rho}\, d\rho$$

$$= \frac{\sin[\alpha(u_o x + v_o y) - q\pi]}{\alpha(u_o x + v_o y) - q\pi}\, e^{-j[(u_o x + v_o y) - \frac{q\pi}{\alpha}]}.$$

APPENDIX C

The Single Sideband Interferometer

For the single sideband interferometer the system output corresponding to (3) is

$$P(u) = \frac{\sin\left[\left(\frac{\pi B}{\omega_o}\right) z_o u\right]}{\frac{\pi B}{\omega_o} z_o u} \cos\left[\left(1 \pm \frac{\omega_1}{\omega_o}\right) z_o u\right]$$

where the + and - signs in the cosine correspond to the lower and upper sideband cases, respectively. The spatial frequency distributions are

$$r(z) = \frac{\omega_o}{4\pi B z_o} e^{j u_o z}, \text{ for } \left| |z| - \left(1 \pm \frac{\omega_1}{\omega_o}\right) z_o \right| < \frac{\pi B}{\omega_o},$$

$$= 0, \text{ otherwise.}$$

The lower sideband spectrum is of width $2\frac{\pi B}{\omega_o}$ and is centered at $z = \left(1 - \frac{\omega_1}{\omega_o}\right) z_o$, while the upper sideband spectrum of the same width is centered at $z = \left(1 + \frac{\omega_1}{\omega_o}\right) z_o$.

The equivalent monochromatic interferometer consists of an isotropic element and a uniform linear aperture of length $\frac{2\pi B}{\omega_o} z_o$. The baselines are $\left(1 - \frac{\omega_1}{\omega_o}\right) z_o$ and $\left(1 + \frac{\omega_1}{\omega_o}\right) z_o$ for the lower and upper sidebands, respectively.

As in the double sideband system, the broadening of the spatial frequency passband with lengthening baselines permits one to reduce the number of sampling intervals. The formulas corresponding to (13) and (14) are given below:

$$\bar{n} = \left[\frac{1 \pm \frac{\omega_1}{\omega_o} - \alpha}{2\alpha} \right] , \quad \alpha = \frac{2\pi B}{\omega_o} , \tag{14a}$$

$$z_n = \frac{n}{1 \pm \frac{\omega_1}{\omega_o}} \frac{\lambda_o}{2} , \text{ for } n < \bar{n} .$$

$$z_n = \left(\frac{1 \pm \frac{\omega_1}{\omega_o} + \alpha}{1 \pm \frac{\omega_1}{\omega_o} - \alpha} \right)^{n - \bar{n}} \left(\frac{\bar{n}}{1 \pm \frac{\omega_1}{\omega_o}} \right) \frac{\lambda_o}{2} , \text{ for } n > \bar{n} . \tag{13a}$$

The negative sign indicates the lower sideband case. If N baselines are used the number of half wavelength intervals is

$$M_{\pm} = \left(1 \pm \frac{\omega_1}{\omega_o} \right) \left(\frac{1 \pm \frac{\omega_1}{\omega_o} + \alpha}{1 \pm \frac{\omega_1}{\omega_o} - \alpha} \right)^{N - \bar{n}} \frac{\bar{n}}{1 \pm \frac{\omega_1}{\omega_o}} .$$